1989Ap&SS.154..119N

POLARIZATION OF RESONANCE LINES FORMED IN EXTENDED SPHERICAL ATMOSPHERES

K. N. NAGENDRA

Indian Institute of Astrophysics, Bangalore, India

(Received 26 October, 1988)

Abstract. The problem of polarization of the resonance lines formed in extended spherical atmospheres is studied in detail. In this paper, the atmosphere is assumed to be at rest. The basic problem of resonance line polarization in spherical atmospheres as compared to the conventionally used plane-parallel atmospheres, is studied in Nagendra (1988). Our main interest in this paper is to understand the behaviour of polarized radiation fields in extended model spherical atmospheres so that some constraints can be placed on the model parameters in the modelling work conected with observations of polarization across resonance lines. A comparison of polarized lines formed under three kinds of line-scattering mechanisms is also made. They are CS = coherent scatteirng, CRD = complete redistribution, and PRD = partial frequency redistribution which, in the increasing order of generality, provide a good approximation in the two-level atom approach, to the resonance line polarization. The dependence of polarization on the opacity laws, extendedness and on optical depth is studied in detail. The distribution of line intensity and polarization across the visible disk of an extended model stellar atmosphere is studied, in view of the possible disk-resolved observations in future, of the extended atmospheres of the stars.

1. Introduction

The theory of resonance line polarization was first successfully used by Stenflo *et al.* (1980, and references given therein) in the study of solar resonance lines. In these studies, either CS or CRD were generally used as the line-scattering mechanisms which are reasonably good approximations in the line wing or the line core, respectively. The importance of PRD as a realistic and general line-scattering mechanism, was clearly demonstrated by Dumont *et al.* (1977) and Rees and Saliba (1982). They have used angle-averaged PRD functions. Faurobert (1987, 1988) studied these problems in detail using angle-dependent PRD functions. Such calculations have been useful in the modelling of resonance line polarization observed in solar prominences. McKenna (1984, 1985) has computed polarization profiles using various PRD functions as well as realistic model stellar atmospheres. He has also presented the polarized profiles computed for non-spherical stars. All the calculations mentioned above have used plane-parallel (PP) approximation in solving the relevant radiative transfer problem. We have solved the problem of resonance line polarization with PRD functions in spherically-symmetric (SS) atmospheres (Nagendra, 1988). Elastic and inelastic collisions play an important role in the generation of line polarization in resonance and subordinate lines. In an important paper, Domke and Hubený (1988) have given a general redistribution matrix for including the collisions, starting from the previous calculations by Ballagh and Cooper (1977). The uncertainties in the inclusion of collisions now being removed, it would be more fruitful to include them in a parametrized way in subsequent theoretical work on polarized line transfer calculations. Streater *et al.* (1988) also have

Astrophysics and Space Science **154**: 119–142, 1989.
© 1989 *Kluwer Academic Publishers. Printed in Belgium.*

© Kluwer Academic Publishers • Provided by the NASA Astrophysics Data System

1989Ap&SS.154..119N

developed a quantum formulation of this problem including collisions. The scalar PRD transfer problem in spherical atmospheres is well studied (see Linsky, 1988; and Mihalas, 1978, for a review of this problem). The analogous problem in polarized transfer is useful in practical applications – particularly in modelling the resonance line polarization observed in supernova atmospheres. Such high-resolution studies on polarization observed across the P-Cygni type intensity profiles, formed in the expanding atmospheres of SN 1987 A has been published recently in an important paper by Cropper *et al.* (1988). The polarization in a resonance line arises due to coherent scattering in the rest frame of the atom. The basic theory of this process in a two-level atom model, and the relevant transfer equation are given in Chandrasekhar (1960). Since the PRD function $R_{\mathrm{II-A}}(x, x')$ in Hummer's notation represents the same mechanism, naturally the use of $R_{\mathrm{II-A}}(x, x')$ or more correctly $R_{\mathrm{II}}(x, \mu, x', \mu')$ is required in the PRD vector transfer calculations. To treat the line polarization in subordinate lines such as Hα, the $\mathbf{R}_{\mathrm{V}}(x, \mu, x', \mu')$ is required. In a PRD problem, to a good approximation, we can use the hybrid model suggested by Rees and Saliba (1982) in separating the angle and frequency coupling in the redistribution matrix occurring in the scattering integral (see also Nagendra, 1988). In the next section we describe the relevant equations retaining the same notation as Nagendra (1988) where they are described in detail. In the subsequent sections the results of the calculations are described.

2. The Spherically-Symmetric Vector Transfer Equations for Line Polarization

We employ the Stokes parameters I_l and I_r to characterize the polarization state of the diffuse radiation field following Chandrasekhar (1960). $I = I_l + I_r$ is the usual specific intensity of the scalar transfer equation. $Q = I_l - I_r$ is the Stokes parameter. $p = Q/I$ is the degree of linear polarization of the radiation field. In azimuthally-asymmetric problems – e.g., the irradiance of the atmosphere by a unidirectional beam of radiation – we need to solve the coupled transfer equation for $(I_l I_r U)^T$ using a 3-dimensional redistribution matrix. The Stokes V parameter however, transfers independently (decoupled from other Stokes parameters). The transformation between the redistribution matrix derived in a density matrix formalism and the Stokes vector formalism is clearly explained in Domke and Hubený (1988). See Nagendra and Peraiah (1985a, 1987) regarding this straightforward transformation in any vector transfer problem. The two-level atom standard NLTE transfer equation in spherical symmetry is given by

$$\mu \frac{\partial}{\partial r} \mathbf{U}(x, \mu, r) + \frac{1-\mu^2}{r} \frac{\partial}{\partial \mu} \mathbf{U}(x, \mu, r) =$$
$$= k^L(\beta + \phi(x)) \left[\mathbf{S}(x, \mu, r) - \mathbf{U}(x, \mu, r)\right], \tag{1}$$

where $\mathbf{U}(x, \mu, r) = 4\pi r^2 \mathbf{I}(x, \mu, r)$ is the Stokes specific intensity vector at the frequency point $x = (\nu - \nu_0)/\Delta\nu_{\mathrm{D}}$ in the line, directed at an angle $\theta = \cos^{-1}\mu (\mu \in [0, 1])$ to the radius vector at the radial point r, in the standard notation (see Mihalas, 1978). ν_0 is

© Kluwer Academic Publishers • Provided by the NASA Astrophysics Data System

1989Ap&SS.154..119N

the line center frequency. The Doppler width is given by $\Delta\nu_D = \nu_0/c\sqrt{2kT/M}$. The quantity β is the ratio k^C/k^L of the continuous opacity per unit interval of x to the frequency integrated line opacity k^L. The optical-depth scale is given by $d\tau = -k^L(r)\,dr$. The quantity $\phi(x) = H(a, x)/\sqrt{\pi}$ is the absorption profile function. $H(a, x)$ is the Voigt function. a is the damping parameter. The source vector $\mathbf{S}$ is given by

$$\mathbf{S}(x, \mu, r) = \frac{\phi(x)\mathbf{S}^L(x, \mu, r) + \beta\mathbf{S}^C(r)}{(\beta + \phi(x))} . \tag{2}$$

$\mathbf{S}^C(r) = 0.5\mathbf{B}'(r)\mathbf{1}$; $\mathbf{1} = (1, 1)^T$, is the continuous source vector. $B'(r) = 4\pi r^2$. $B(T(r))$ is the Planck function assumed as constant over the bandwidth of the line. $\mathbf{S}^L(x, \mu, r)$ is the line source vector given by

$$\mathbf{S}^L(x, \mu, r) = \begin{bmatrix} S_l^L(x, \mu, r) \\ S_r^L(x, \mu, r) \end{bmatrix} = \frac{(1-\varepsilon)}{\phi(x)} \int_{-\infty}^{+\infty} dx' \int_{-1}^{+1} \mathbf{R}(x, \mu, x', \mu')\mathbf{U}(x', \mu', r)\, d\mu' + \frac{\varepsilon}{2} B'(r)\mathbf{1} . \tag{3}$$

In the equation above ε is the probability per scatter that the line photon is destroyed through collisional de-excitation in the two-level atom. $\mathbf{R}(x, \mu, x', \mu')$ is the redistribution matrix which contains the essential physics of line-scattering mechanism. Employing the Rees–Saliba prescription for angular and frequency decoupling, it can be written as

$$\mathbf{R}(x, \mu, x', \mu') = \mathbf{P}(\mu, \mu')R(x, x') , \tag{4}$$

where the angular phase matrix $\mathbf{P}(\mu, \mu')$ which contains the angular information in the scattering event is given by

$$\mathbf{P}(\mu, \mu') = \tfrac{3}{8}E_1 \begin{bmatrix} 2(1-\mu^2)(1-\mu'^2) + \mu^2\mu'^2 & \mu^2 \\ \mu'^2 & 1 \end{bmatrix} + \frac{(1-E_1)}{4}\begin{bmatrix} 1 & 1 \\ 1 & 1 \end{bmatrix} . \tag{5}$$

The factor $(1 - E_1)$ is a measure of depolarization caused by virtue of the level structure. E_1 depends on the angular momentum quantum numbers of both the levels involved in the transition. In all our computations we have employed $E_1 = 1$. The redistribution function is given by the following expressions, with the corresponding line-scattering mechanisms indicated against them.

$$\text{CS:} \quad R(x, x') = \delta(x - x')\phi(x') , \tag{6}$$

$$\text{CRD:} \quad R(x, x') = \phi(x)\phi(x') , \tag{7}$$

$$\text{PRD:} \quad R(x, x') = R_{\text{II–A}}(x, x') . \tag{8}$$

The angle-averaged partial redistribution function is given by

$$R_{\text{II–A}}(x, x') = \pi^{-3/2} \int_{1/2(|\tilde{x} - \underline{x}|)}^{\infty} e^{-u^2}\left[\tan^{-1}\left(\frac{\underline{x} + u}{a}\right) - \tan^{-1}\left(\frac{\tilde{x} - u}{a}\right)\right] du , \tag{9}$$

© Kluwer Academic Publishers • Provided by the NASA Astrophysics Data System

1989Ap&SS.154..119N

where $\tilde{x} = \max(x, x')$ and $\underset{\sim}{x} = \min(x, x')$. This function refers to the model atom where the upper level is naturally broadened and the lower level has a zero width. We have employed the conventional boundary conditions which are given by

$$\left.\begin{aligned} \mathbf{U}(x, \mu, \tau = T) &= 0.5\,, \\ \mathbf{Q}(x, \mu, \tau = T) &= 0\,, \end{aligned}\right\} \tag{10}$$

at $\tau = T$ or $r = 1$; and

$$\left.\begin{aligned} \mathbf{U}(x, -\mu, \tau = 0) &= 0\,, \\ \mathbf{Q}(x, -\mu, \tau = 0) &= 0\,, \end{aligned}\right\} \tag{11}$$

at $\tau = 0$. Equation (10) represents an unpolarized diffuse radiation field incident on the lower boundary and Equation (11) represents that no radiation is incident on the external free surface. The basic method of computation for the scalar line transfer problem is described in Peraiah (1984). The details about using this method to polarized continuum and line transfer problems are given in Nagendra and Peraiah (1984, 1985a, b) and Nagendra (1987, 1988). There are also two classes of results presented in this paper. The quantities $I(x, \mu, r)$ and $p(x, \mu, r)$ represent the diffuse radiation field intensity and polarization obtained by a solution of the vector transfer equation in spherical symmetry. $I(x, h)$ and $p(x, h)$ represent the corresponding quantities at different points on the visible stellar disk. The later can be obtained after an integration along the line-of-sight using the spherically-symmetric source functions obtained in the former calculation. This line-of-sight integration is a simple task, and takes care of the occultation by stellar core and large emission contributions from the extended side lobes. Our models are parametrized by the following parameters: R is the outer radius of the spherical shell-like atmosphere. $R_c = 1$ is the inner core radius. T is the frequency integrated optical thickness of the shell. The central core is an emitting source (e.g., like the stellar photosphere). Hence, the inner boundary condition employed is $\mathbf{U}(x, \mu, T) = 0.5$. The PP limit is obtained by taking $R = 1$. In the examples presented in this paper, we have employed the following opacity laws:

$$k^L(r) = K\,; \qquad \tau^L(r) = K(R - r)\,, \qquad K = \frac{T}{(R-1)}\,, \tag{12}$$

representing a constant opacity spherical shell; or

$$k^L(r) = Kr^{-2}\,; \qquad \tau^L(r) = \frac{RT}{(R-1)}\left[\frac{1}{r} - \frac{1}{R}\right], \qquad K = \frac{RT}{(R-1)}\,, \tag{13}$$

representing an inverse-square opacity variation in the spherical atmosphere. The continuum optical-depth scale is given by $\tau^C(r) = \beta\tau^L(r)$. The Planck function which acts as the continuum thermal source of radiation in the atmosphere is chosen to be $B'(r) = 1$. This corresponds to an isothermal atmosphere in all the models shown in this paper. The bandwidth of the line is selected such that the monochromatic optical-depth $T_x = T(x) = T\phi(x)$ at the line-wing frequencies satisfy the condition $T(x_{\max}) \ll T$.

© Kluwer Academic Publishers • Provided by the NASA Astrophysics Data System

1989Ap&SS.154..119N

3. Results and Discussion

3.1. Effect of the extendedness (R) of the atmosphere on the emergent polarization profiles

In the series of cases presented in Figures 1–3 the effects of extendedness are discussed taking the three approximations to the scattering mechanism: namely, CS, CRD, and PRD. The angular distributions of emergent diffuse radiation intensity and polarization are also shown. The models are characterized by inverse-square opacity variation $k(r) = Kr^{-2}$ and a constant Planck function $B'(r) = 1$ over the depth. The quantity μ_1 corresponds to nearly transverse direction and μ_3 to nearly normal direction of propagation with respect to the symmetry axis, viz., the local normal in a PP medium ($R = 1$) and the radius vector in a SS medium ($R \neq 1$). The atmosphere is effectively thick ($\varepsilon T > 1$); hence, the photon escape probability is low. First we will take up Figures 1(a–c). For these cases, the line-scattering mechanism is CRD. The polarization profiles for all the models $R = 1$, 3, and 10 have negative maxima at the line center and a small positive peak around $x \simeq 2$ before reaching almost zero-value in the near-wing region itself. This is mainly due to the large value of continuum opacity adopted by us, which being isotropic and non-scattering, naturally drives the polarization of the diffuse radiation field to zero values. The value of the specific intensities in SS models $R = 3$, 10 are much smaller than the PP model. The reason for this is obviously the characteristic behaviour of the radiative transfer solution in spherical geometry. They are as follows: (i) The bias in scattering towards the larger radius in spherical geometry. Note that in PP geometry, a photon goes with equal probability to larger or smaller depths. (ii) The dilution of diffuse radiation field in spherical geometry. The dilution factor is given by

$$2W = J(r = R)/J(r = 1) = [1 - (1 - {}^1/R^2)^{1/2}] . \tag{14}$$

It is important to note that W rapidly decreases from the value of unity (for $R = 1$), even for a small deviation from planar limit. However, this trend saturates for larger values of R. This is the reason for marked difference between $R = 1$ and $R = 3$ solutions and only a small difference between $R = 3$ and $R = 10$ solutions. (iii) The peaking of the radiation into the radial direction as one goes out, particularly in optically thin extended spherical atmospheres. This is purely a curvature effect. This mainly causes numerical difficulties by demanding finer angular grid in the transfer calculations in spherical geometry. These three characteristics are always the main reasons for the difference of SS solutions from PP solutions, irrespective of other details. Note also that SS solutions approach PP solutions as $\mu \to 1$. The $B'(r) = 1$ case corresponds to an increased thermal photon creation rate towards the surface, because of which the dilution effect is disguised. The polarization is higher at the line-center for SS models than the PP models.

An intercomparison among Figures 1(a–c) shows that the difference between $R = 3$ and $R = 10$ intensity profiles decreases as we go from μ_1 to μ_3. Also the difference between PP and SS solutions decreases. The saturation to the continuum level occurs

© Kluwer Academic Publishers • Provided by the NASA Astrophysics Data System

1989Ap&SS.154..119N

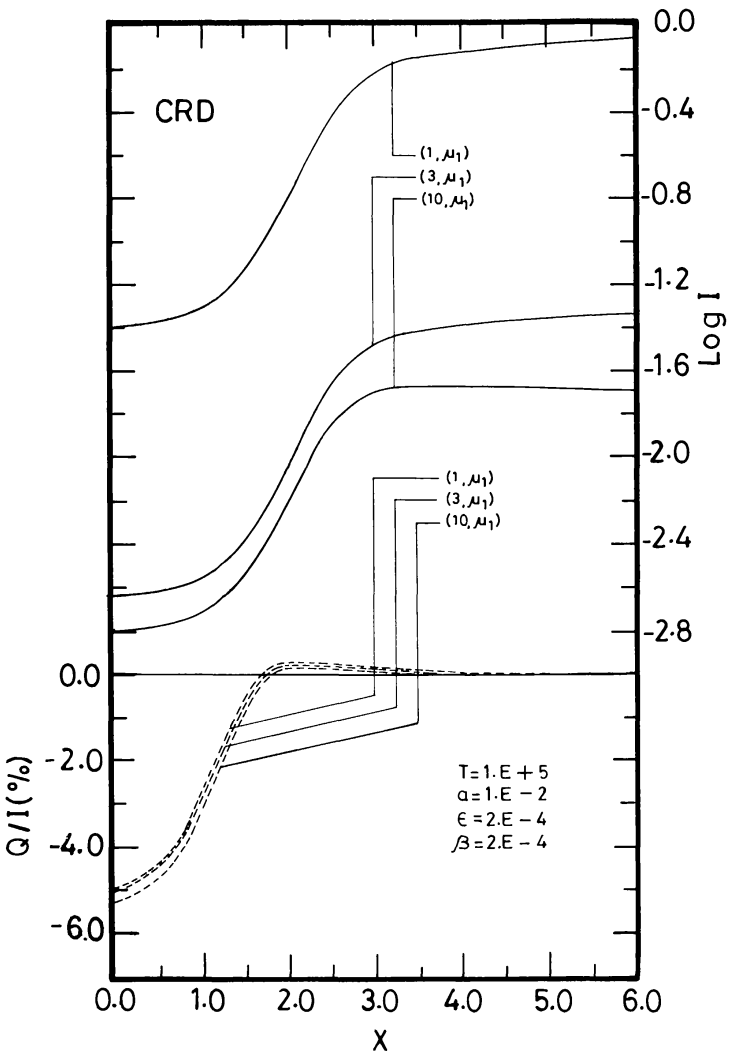

Fig. 1a. Emergent specific intensity I (solid lines) and linear polarization Q/I (dashed lines) in plane-parallel ($R = 1$) and spherically-symmetric ($R \neq 1$) configurations for the given atmospheric model (T, a, ε, β) for the direction $\mu_1 = 0.11$. The line-scattering mechanism is complete redistribution (CRD) in frequency. The symbols are described in the text. Note the effect of extendedness (R). The angular (μ) dependence can be understood by a comparison of Figures 1(a), 1(b), and 1(c).

closer to the near-wing frequencies for μ_3 than for μ_1. As expected the degree of polarization over the entire bandwidth decreases as we go from μ_1 to μ_3. But it is important to note that the frequency position of the positive polarization peak shifts towards the line core as we go from μ_1 to μ_3. The intensity profiles clearly show a limb-darkening at all frequency points in the line in both PP and SS models. The PRD profiles for 3 angles are shown in Figures 2(a–c). The discussion given above for CRD profiles holds true for PRD profiles also. But the important difference is that the frequency position of the positive maxima of polarization is nearly same for all the angles μ_1, μ_2, and μ_3. Another basic difference is that the amount of positive polarization in the line wings is more in PRD than in CRD, particularly for smaller extensions ($R < 3$).

© Kluwer Academic Publishers • Provided by the NASA Astrophysics Data System

1989Ap&SS.154..119N

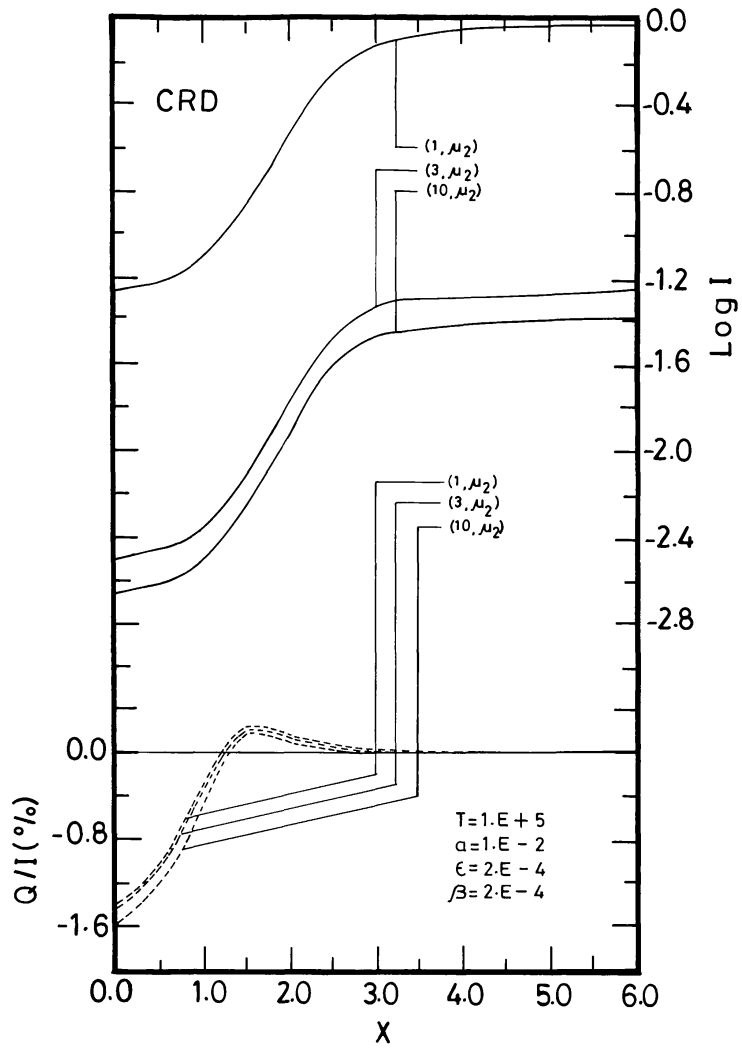

Fig. 1b. Same as Figure 1(a), but for the direction $\mu_2 = 0.5$.

The CS profiles are shown in Figures 3(a–c). It is clearly seen that the two characteristics mentioned above for PRD, are more strongly manifested in the case of CS. It is well known that, in general, the PRD line profiles behave like CRD profiles in the line core and like CS profiles in the far wings. This is mainly due to the strong wing coherence exhibited by $R_{\mathrm{II-A}}(x, x')$ redistribution function. The conditions for the importance (dominance) of line-scattering represented by PRD mechanism in the line wings, in the presence of a continuous absorption is given by Hubený (1985). The inequality $\beta \ll a/\pi^2$ represents this condition. With our present choice of parameters ($\beta = 2 \times 10^{-4}$; $a = 10^{-2}$), this inequality is marginally satisfied. Hence, in our profiles, continuum absorption also plays an important role in the wings and, hence, drives the polarization to zero in the wings. A comparison of the nature of the redistribution functions for CS, CRD, and PRD shows that the number of scatterings at any frequency point x is more for PRD than for CRD. Moreover, the scattering according to $R_{\mathrm{II-A}}(x, x')$ in the line wings, is frequency diffusive in nature, with the photon diffusion

© Kluwer Academic Publishers • Provided by the NASA Astrophysics Data System

1989Ap&SS.154..119N

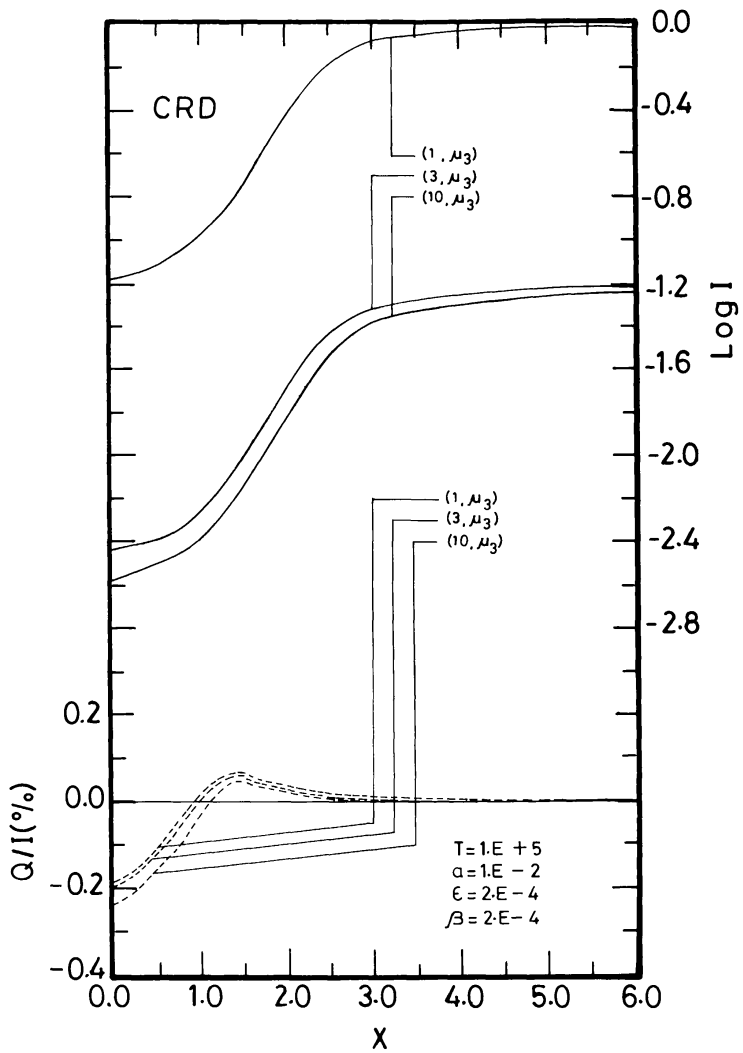

Fig. 1c. Same as Figure 1(a), but for the direction $\mu_3 = 0.89$.

directed towards the line core. The polarization, than the scalar specific intensity in the line, depends more sensitively on these matters. The line polarization is a sensitive function of the source function gradient set-up in the atmosphere. The polarized source vector is even more sensitive function of physical parameters of the models, than the usual scalar source function. However, for this same reason, polarization is a more sensitive probe of the stellar atmosphere, only if the polarization data is interpreted properly. The CS is an idealistic line-scattering mechanism. We have shown the CS profiles in Figures 3(a–c) only to get an idea of the maximum amount of polarization obtainable in a given model. The CS source function is larger compared to the CRD/PRD source functions throughout the atmosphere excepting in the outermost part of the atmosphere. This characteristic is stronger in the SS model than in the PP models. This also indicates enhanced multiple scattering in CS and a weaker coupling to the thermal radiation field. Clearly there is no coupling of any two frequencies in the line, in the CS scattering integral. Thus, in a coherently scattering medium, the extension

© Kluwer Academic Publishers • Provided by the NASA Astrophysics Data System

1989Ap&SS.154..119N

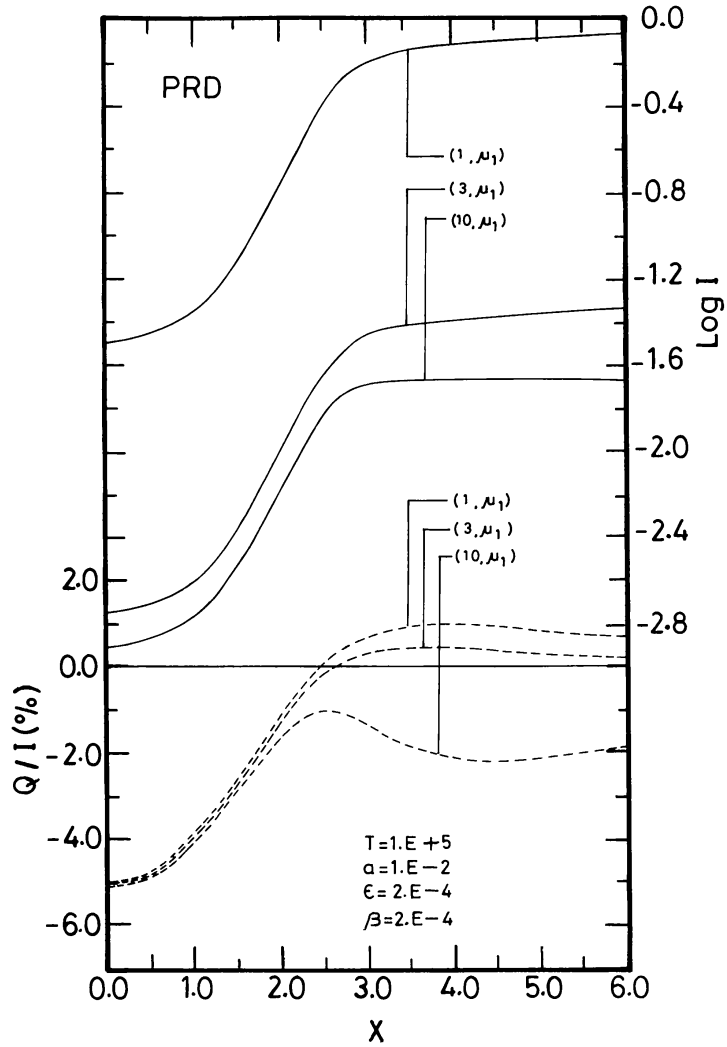

Fig. 2a. Same as Figure 1(a), but now the line-scattering mechanism is partial redistribution (PRD) in frequency. See also Figures 1(a–c).

appears to enhance negative content of polarization throughout the line profile particularly so in the line wings.

A general comparison of Figures 1–3 reveals that, for the angle μ_1, CS/PRD/CRD intensity profiles have central depth in the decreasing order. For the other two angles, μ_2 and μ_3, PRD intensity profiles are slightly deeper than the CS profiles, but CRD-profiles once again are less deeper than both CS and PRD profiles. The behaviour of the polarization profiles formed under CS/PRD/CRD is quite similar in the line core, with a maxima followed by a rise towards the zero-polarization line. The width of the central polarization peak shows a decreasing trend when going from CS to PRD and CRD. The CS and PRD polarization profiles in the highly extended model $R = 10$ show double negative peaks, one at the line center and the other somewhere near $x \sim 4.5$. The reason for this similarity is obviously, the wing coherence of the $R_{\mathrm{II-A}}(x, x')$ partial redistribution. However, the positions of the peaks in the wing are slightly different for

© Kluwer Academic Publishers • Provided by the NASA Astrophysics Data System

1989Ap&SS.154..119N

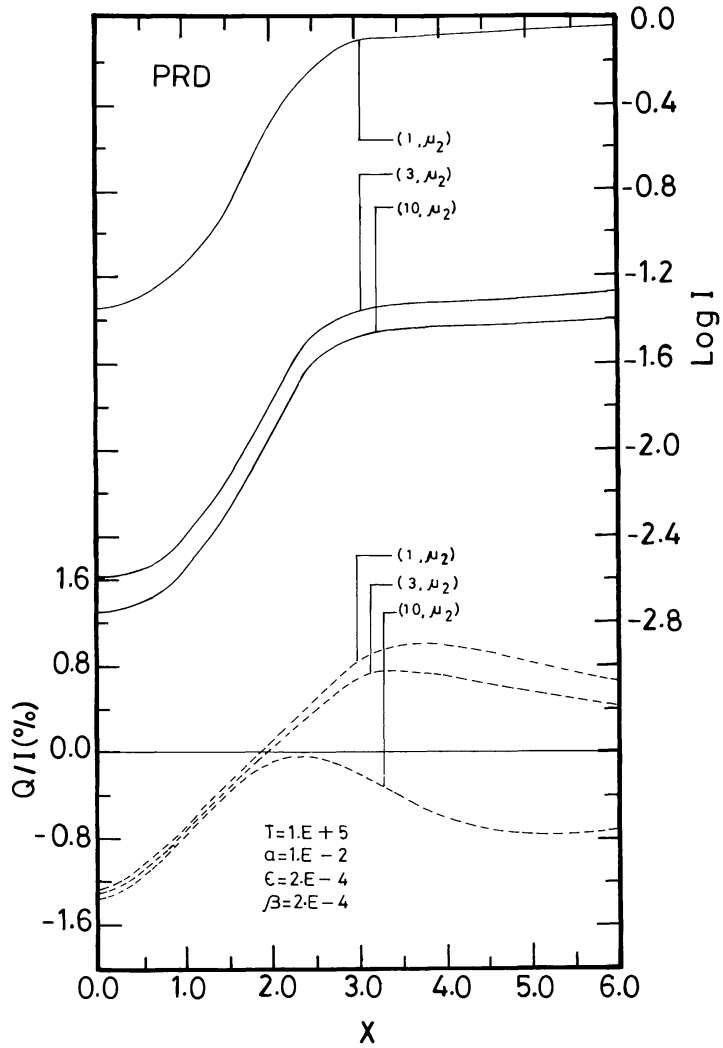

Fig. 2b. Same as Figure 2(a), but for the direction $\mu_2 = 0.5$.

CS and PRD. The apparent convergence of polarization in the $x \simeq 6$ region for all the three mechanisms is mainly because of the large β-value of our models. They actually differ widely in the absence of a continuum, with PRD going to CS values of polarization only in the very far wings. However, in actual stellar atmospheres, the continuum opacity is important and actually corresponds to the kind of values we have selected in this paper.

3.2. Effect of opacity variations and optical depths on the polarization profiles

In this section we discuss the effects mentioned above, using the CS, CRD, and PRD line-scattering mechanisms. This helps us to get an idea of among which these mechanisms are more sensitive to the opacity law and line center optical-depth parameters. Equations (12) and (13) represent a constant opacity model and inverse-square opacity models in computing the profiles presented in Figures 4–6.

© Kluwer Academic Publishers • Provided by the NASA Astrophysics Data System

1989Ap&SS.154..119N

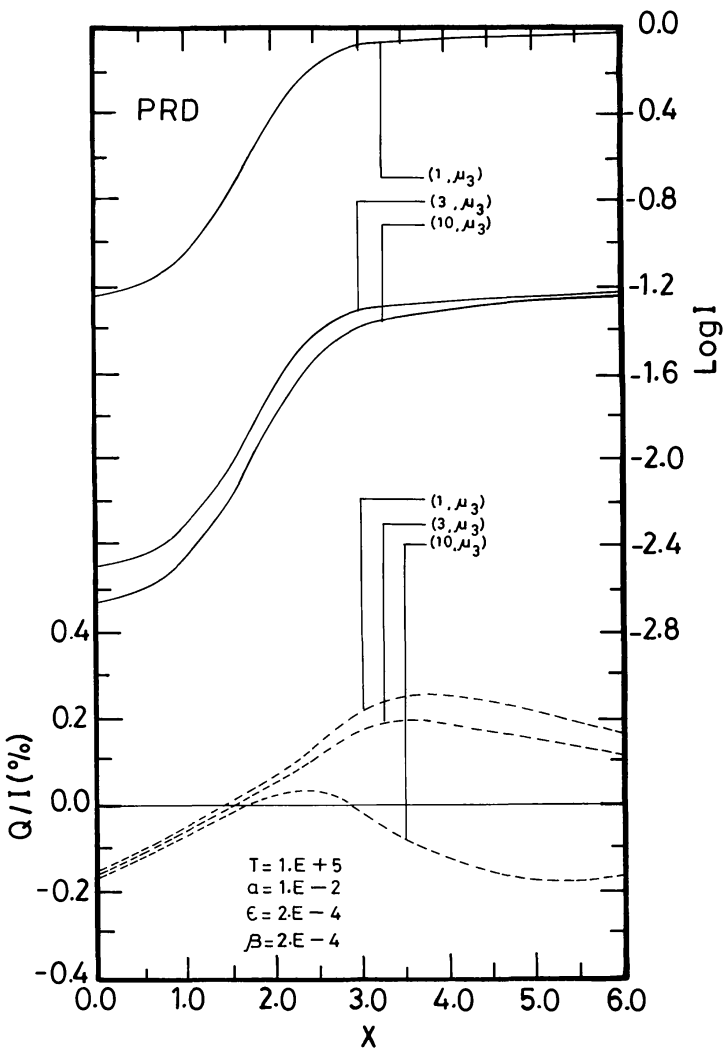

Fig. 2c. Same as Figure 2(a), but for the direction $\mu_3 = 0.89$.

The sphericity effects clearly manifest themselves for inverse-square opacity law than the constant opacity law, the reason being that the bias in scattering mentioned earlier, is particularly important for the inverse-square opacity model. Since the photon mean-free paths in the outward direction are larger than in the inward direction, in the inverse-square opacity model, the bias in scattering is very effective in the outermost layers. First let us consider $T = 10^4$ models. The $T = 10^4$ model is optically moderately thick ($(aT)^{1/3} \approx 4.6$) and effectively moderately thick ($\varepsilon T = 2$). In the inverse-square opacity model (dashed lines), there is a small wing emission around $x \simeq 3$. Since the opacity is highest in the layers closest to the stellar core, the wing photons are easily absorbed, leading to a relative depression of the far-wing intensity profile. The CRD intensity profile in this case is depressed more compared to CS and PRD which have nearly equal values. The polarization profile of CRD is not much affected. But the PRD and CS polarization profiles are drastically depressed and develop a negative polarization peak in the wing around $x \simeq 4$. It is important to ntoe that the near-wing emission

© Kluwer Academic Publishers • Provided by the NASA Astrophysics Data System

1989Ap&SS.154..119N

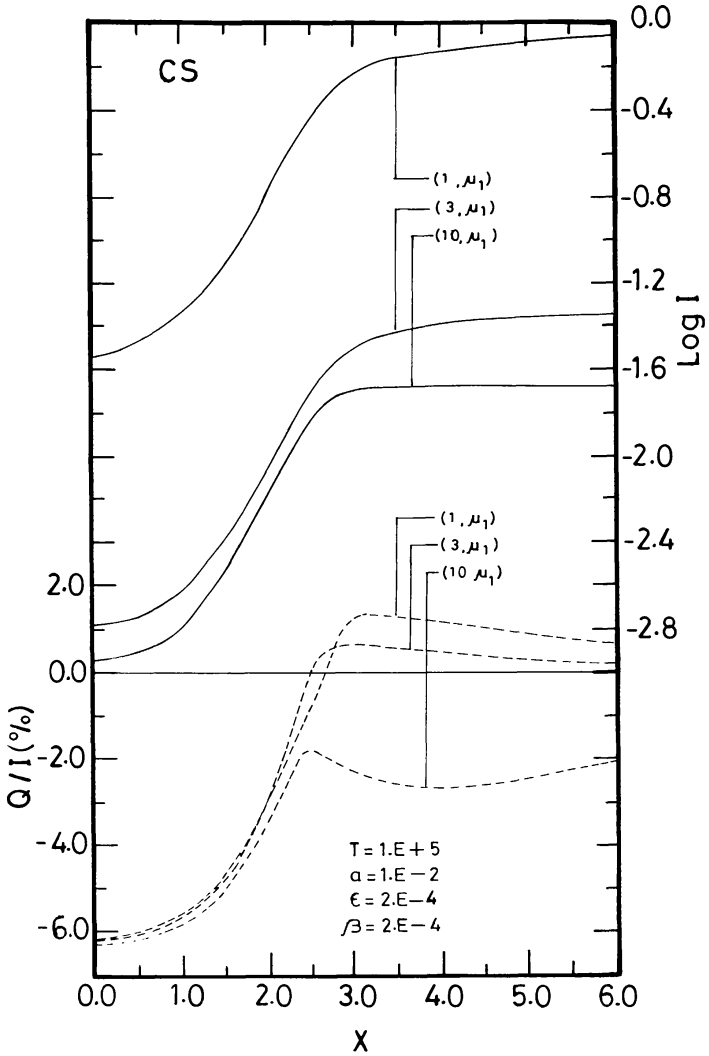

Fig. 3a. Same as Figure 1(a), but now the line-scattering mechanism is coherent scattering (CS) in frequency. See also Figures 1(a–c) and Figures 2(a–c).

peaks in the intensity profiles do not correspond to the positive polarization peaks in CRD cases (Figure 4). The later are shifted towards the line core. In the constant opacity models (full lines), the intensity profiles are deeper than those corresponding to the inverse-square opacity. Also, the intensity profiles do not show the near-wing emission; the line-wing intensities reach the continuum level smoothly. Though the polarization profiles exhibit similar behaviour as the corresponding inverse-square opacity cases, they show comparatively larger polarization in the line core, and a smaller polarization in the line wings also varying smoothly. This is because of a smoother source function gradient which obtains in the atmosphere. The characteristics of polarization profiles of CRD/PRD/CS in terms of their width and frequency dependence, etc., are similar to those discussed in the previous section of this paper, where these mechanisms are compared in detail. Now, we will consider $T = 10^5$ models (dot-dashed and dotted curves in Figures 4–6). A comparison of these cases with $T = 10^4$ models gives an idea

© Kluwer Academic Publishers • Provided by the NASA Astrophysics Data System

1989Ap&SS.154..119N

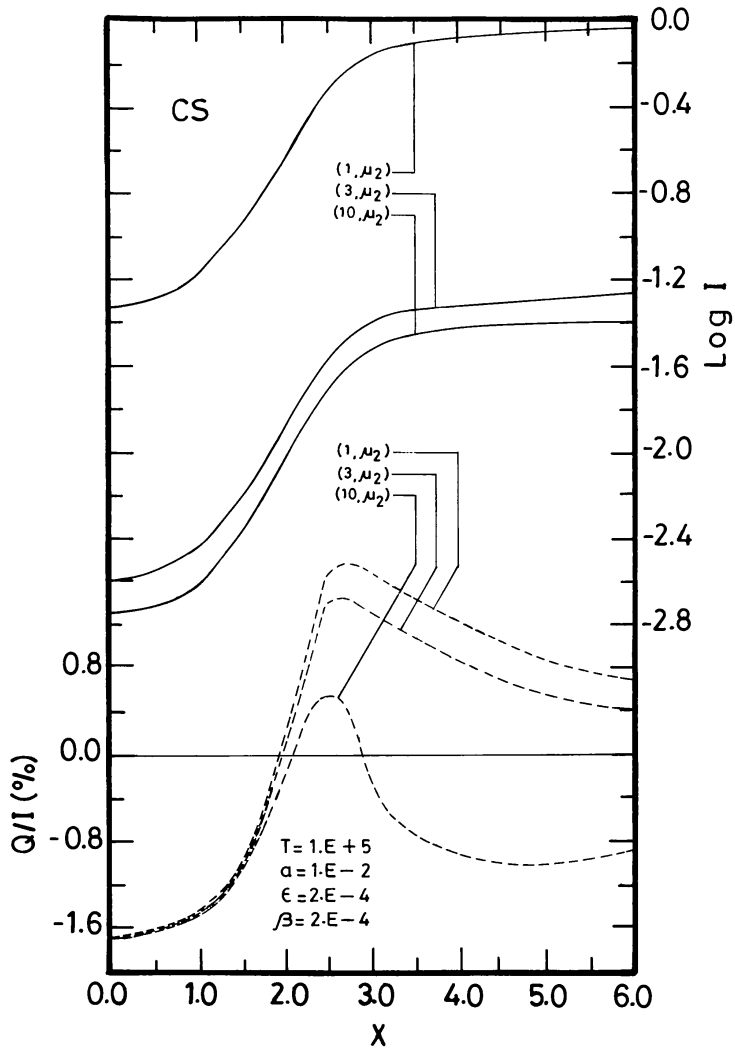

Fig. 3b. Same as Figure 3(a), but for the direction $\mu_2 = 0.5$.

of the role of optical thickness T in the polarization line transfer for a given model. The value of $T = 10^5$ corresponds to optically thick ($(aT)^{1/3} = 10$) and effectively thick ($\varepsilon T = 20$) regime. The continuum optical depth is also high ($T^C = \beta T = 20$). From Figures 4–6 one can see that the increase in optical depth has produced significant changes in the line wings. The line-wing photons are thermalized in the near-wing frequencies itself. The line core is obviously more deeper than those of $T = 10^4$ cases. The difference between the inverse-square opacity cases (dotted lines of Figures 4–6) and constant opacity cases (dot-dashed lines of Figures 4–6) is much less conspicuous in our high optical depth ($T = 10^5$) models. The main reason for this is the line saturation which occurs in optically and effectively thick lines making the emergent profiles rather insensitive to the details of the opacity variation. It is clear that the increase in number of scatterings due to increase in T-value results in the depletion of negatively-polarized photons in the line core. In other words, multiple scattering appears to enhance the positive polarization all over the line – irrespective of the scattering

© Kluwer Academic Publishers • Provided by the NASA Astrophysics Data System

1989Ap&SS.154..119N

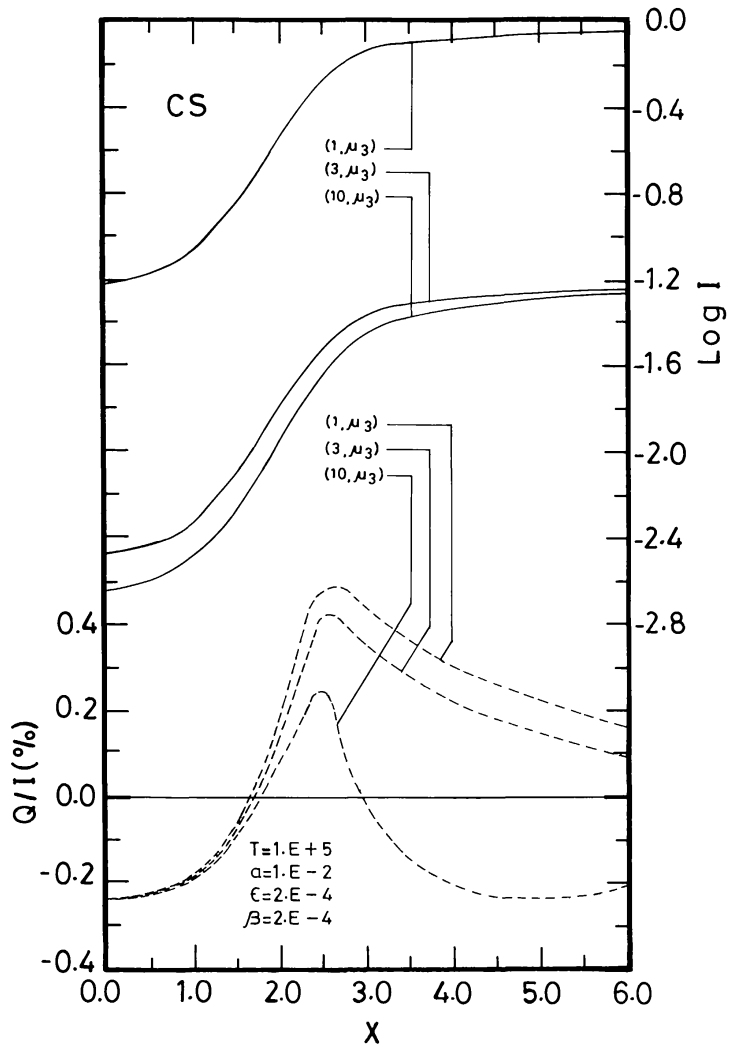

Fig. 3c. Same as Figure 3(a), but for the direction $\mu_3 = 0.89$.

mechanism. Another feature is the narrowing of the intensity and polarization profiles in the $T = 10^5$ case, compared to the $T = 10^4$ case.

The sensitive dependence of the polarization on the optical-depth parameter T is further demonstrated in Figures 7 and 8. There we have shown the angular dependence of the emergent linear polarization at three frequency points in the line profile, for the models indicated in the diagrams. In the low-optical-depth model ($T = 10^4$) shown in Figure 7, the angle dependence is significantly different for the PP case represented by $R = 1$, and the other two SS cases represented by constant and inverse-square opacity laws. This shows that the radiation field is generally more angularly-anisotropic than the $T = 10^5$ case (Figure 8). The degree of angular anisotropy is quite different for the constant opacity and inverse-square opacity models. A comparison of the high-optical-depth model (Figure 8) with Figure 7 clearly indicates that the emergent polarization in high-optical-depth models is generally small in the ling-wing frequencies except for the line center. Also line-wing polarizations are predominantly positive and show larger

© Kluwer Academic Publishers • Provided by the NASA Astrophysics Data System

1989Ap&SS.154..119N

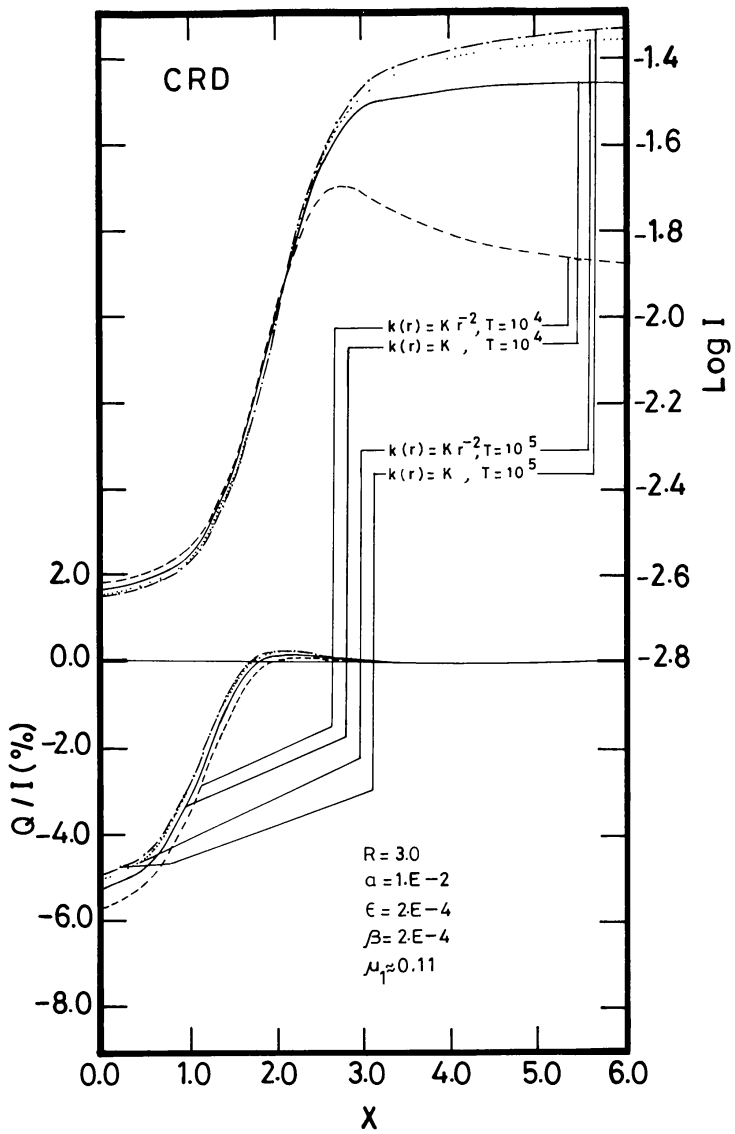

Fig. 4. The effect of opacity variation and the line center optical depth (T) on the emergent intensity (I) and polarization (Q/I) profiles in a spherically-symmetric (R = 3) model. The constant opacity variation $k(r) = K$ and the inverse-square opacity variation $k(r) = Kr^{-2}$ are shown for each value of the optical depth T. The line-scattering mechanism is CRD.

angular isotropy. This characteristic indicates that high optical depths lead to increased thermalization of the line-wing photons, and at the same time make the polarization a less sensitive indicator of the atmospheric extensions and details of the opacity laws.

3.3. Center-to-limb variation of intensity and polarization on the visible disk of extended spherical atmospheres

In this section we discuss the point above using CRD models with different extensions R (Figures 9 and 10). The difference in the center-to-limb behaviour between two kinds

© Kluwer Academic Publishers • Provided by the NASA Astrophysics Data System

1989Ap&SS.154..119N

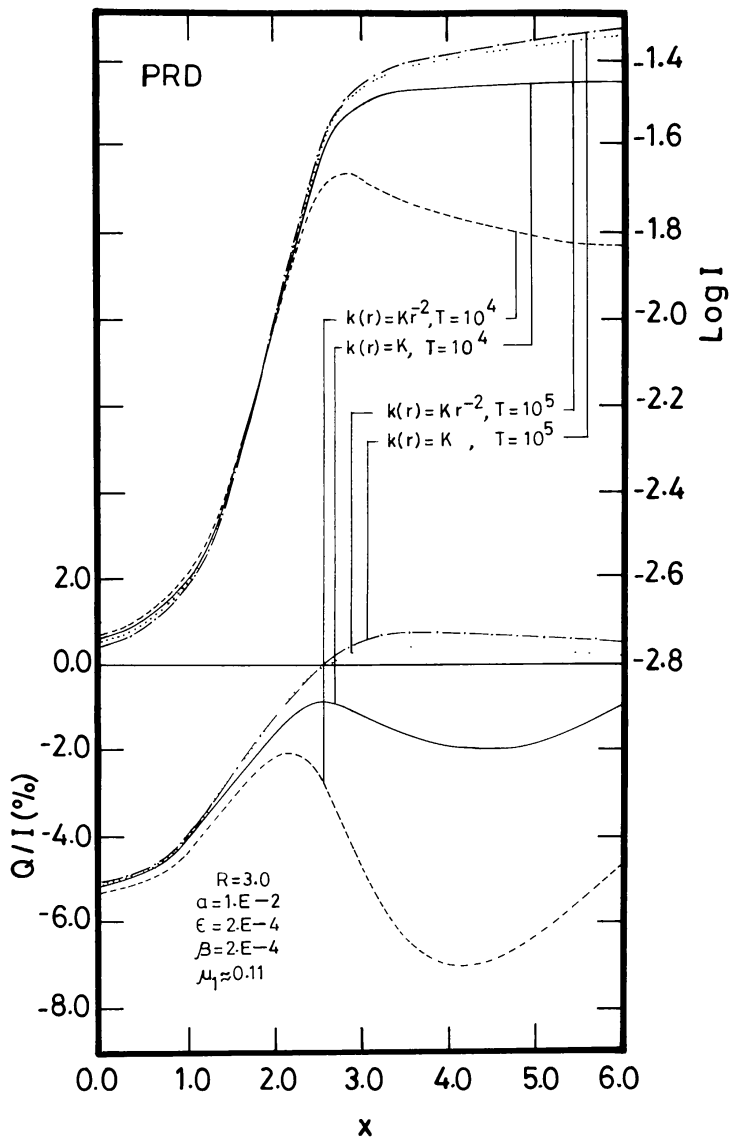

Fig. 5. Same as Figure 4, except for the line-scattering mechanism, which is now the PRD.

of opacity laws in an $R = 3$ model is studied using a CS model (Figures 11 and 12). The line-of-sight specific intensity $I(h)$ and polarization profiles $p(h)$ at different impact parameters h (in other words different radial points on the circular visible disk – which has axially-symmetric distribution of $I(h)$ and $p(h)$ about the central ray joining disk center to the line-of-sight), is computed using a simple formal solution along tangential rays which employ pre-calculated spherically-symmetric source functions of the SS line transfer. Using $I(x, h)$, the disk-integrated observed flux $F(x)$ can be computed. However, the disk-integrated polarization of an SS model is identically zero because of symmetry. When disk-resolved observations of stellar atmospheres become possible in the future, the interpretation requires the computation of $I(h)$ and $p(h)$, or in fact these values at various spatial points, if the atmosphere is non-spherical. As usual, for Figures 9 and 10 $k(r) = Kr^{-2}$ is used. Figure 9 shows the SS emergent intensity and

© Kluwer Academic Publishers • Provided by the NASA Astrophysics Data System

1989Ap&SS.154..119N

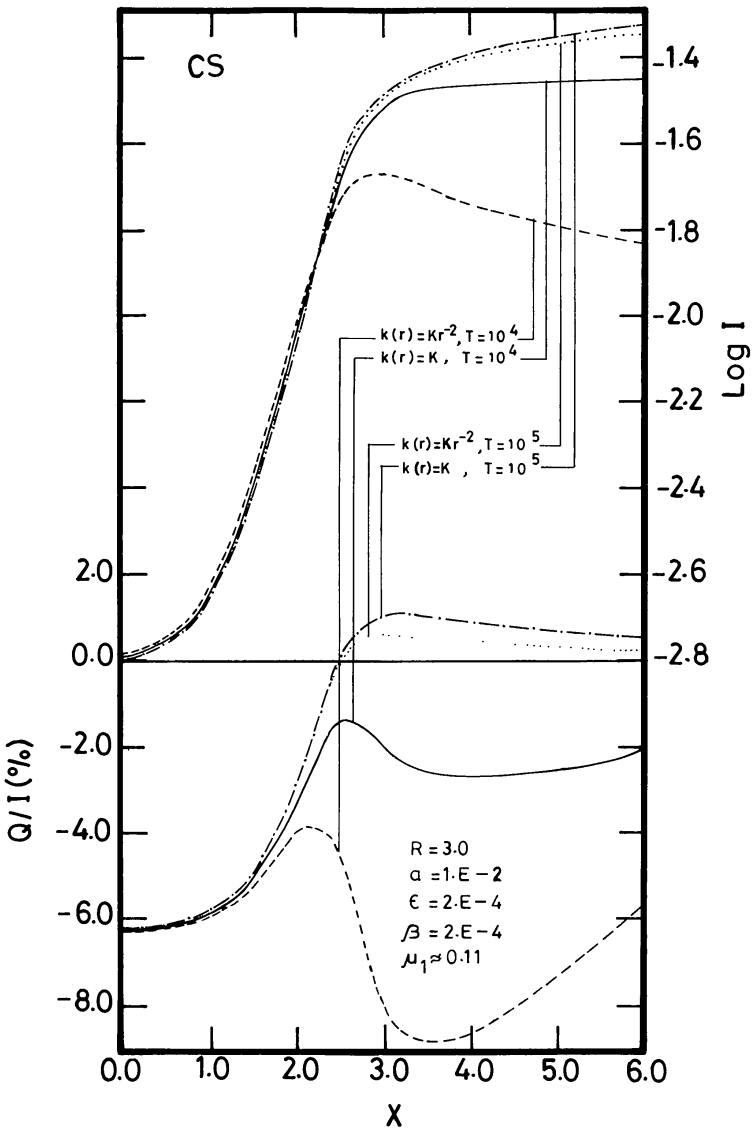

Fig. 6. Same as Figure 4, except for the line-scattering mechanism, which is now CS. See also Figures 4 and 5.

polarization profiles. The intensity profile of the $R = 3$ model is the usual absorption line. But the $R = 10$ intensity profile has a near-wing emission, and is rather wider. The intensity profile of $R = 15$ once again becomes narrow and has a wing emission displaced towards the line center. The polarization profiles of $R = 3$, 10, and 15 are successively of increasing width, with $R = 10$, 15 profiles having negative polarization over the entire width of the line. The disk-integrated profiles shown in the insert give an idea of the extent of the wing emission and the equivalent width of the absorption line. The decrease in the equivalent width of the absorption line as the extension increases, is a well-known result. For highly extended systems the absorption equivalent width will even be negative. The line emission in the entire line profile generally increases with the increasing extension, the emitted photons coming directly from the extended side-lobes of such

© Kluwer Academic Publishers • Provided by the NASA Astrophysics Data System

1989Ap&SS.154..119N

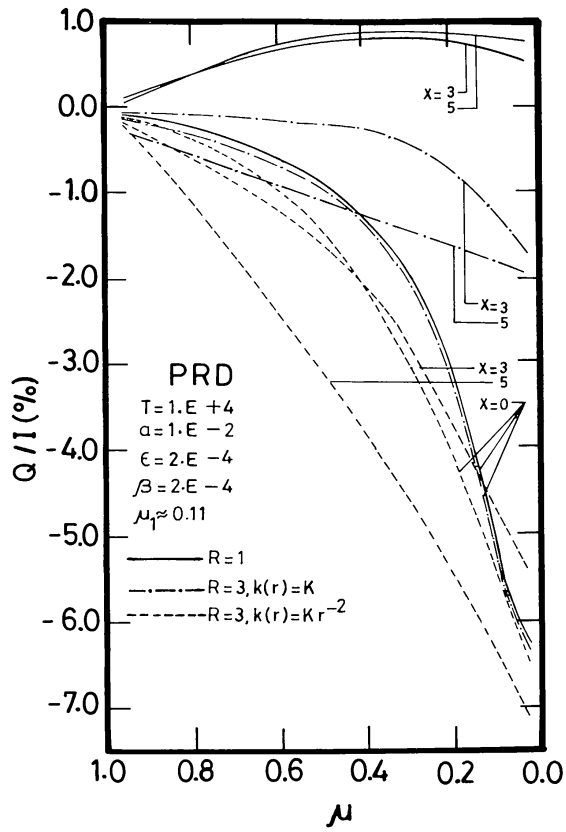

Fig. 7. The angular (μ) dependence of the emergent polarization Q/I in plane-parallel ($R = 1$) and spherically-symmetric ($R = 3$) models, at various frequency points (x) in the bandwidth of the line profile. The angular dependence is shown for two opacity laws in the spherical atmospheres. PRD is the line-scattering mechanism used in these calculations.

models. If, in addition, the atmosphere is expanding, the layers near the stellar core where the line-wing photons are generated, are more exposed.

In Figure 10, we have shown the distribution of intensity $I(h)$ and polarization $p(h)$ on the surface of the three models with $R = 3$, 10, and 15. $I(h)$ and $p(h)$ are shown for only half of the disk, since there is a reflection symmetry about the central plane – the plane containing the line-of-sight and the centre of the disk. When the curves merge closely, some are left out for clarity. The stellar core is assumed to emit a strong, unpolarized, frequency-independent continuum radiation in the bandwidth of the line. This characteristic of the emitting core will dominate the behaviour of all the lines-of-sight intersecting the stellar core ($h \lesssim R_c$). The $I(h)$ for $x = 0$, 0.5, and 1 are almost independent of h. For frequency points $x > 1$, the limb-darkening nature is clearly seen. For line-wing frequency points, the limb-darkening becomes more and more severe in all the three models. The polarization differs, however, somewhat in its behaviour with regard to its dependence on h. The polarization shows weak dependence on h for frequency points in the line core. In the near-wing frequency points the polarization has a stronger dependence, and in the far-wing frequency points once again the dependence on h is weak. As expected, the polarization is nearly zero at the disk centre and

© Kluwer Academic Publishers • Provided by the NASA Astrophysics Data System

1989Ap&SS.154..119N

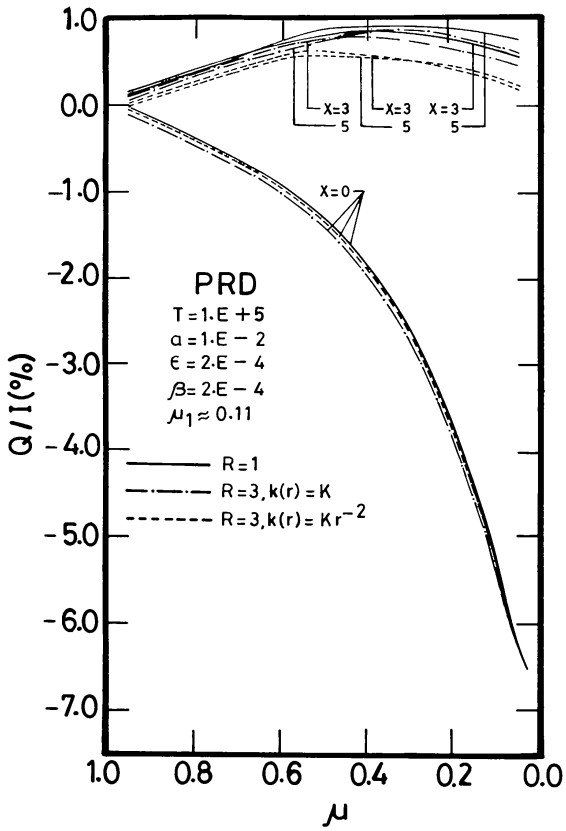

Fig. 8. Same as Figure 7, but for the line-center optical depth whose value is now $T = 10^5$, which represents an optically and effectively thick model.

maximum in the limb of the disk. The polarization is always negative, and varies smoothly across the side lobe.

In Figure 12 we have taken up the comparison of distribution of $I(h)$ and $p(h)$ computed for $k(r) = K$ and $k(r) = Kr^{-2}$ opacity variations in the atmosphere. We have selected the CS model just for the purpose of generating the maximum possible polarization in a given model, so that geometrical effects are clearly separated out. In Figure 11 we have shown emergent SS intensity and polarization profiles. A comparison with PP situation is also shown. The strong frequency-dependence exhibited by the polarization profiles in spherical geometry, and particularly so with the inverse-square opacity law is to be noted. In Figure 12 the intensity profiles are indistinguishable up to $x \simeq 1$. In the frequency range from $x \simeq 1$ to $x \simeq 3$, the stellar disk whose atmosphere has inverse-square opacity variation is brighter. But, for $x > 3$, the limb-darkening becomes steeper in this inverse-square opacity case and, consequently, the limb of the disk is much darker than in the constant opacity case – which shows a somewhat smooth variation in intensity up to 80% of the disk after which there is a rather sharp darkening. The distribution of polarization on the disk of the inverse-square opacity case shows the conventional pattern (see Figure 10). However, the constant opacity case is more interesting. Basically this model produces smaller degree of polarization. More

© Kluwer Academic Publishers • Provided by the NASA Astrophysics Data System

1989Ap&SS.154..119N

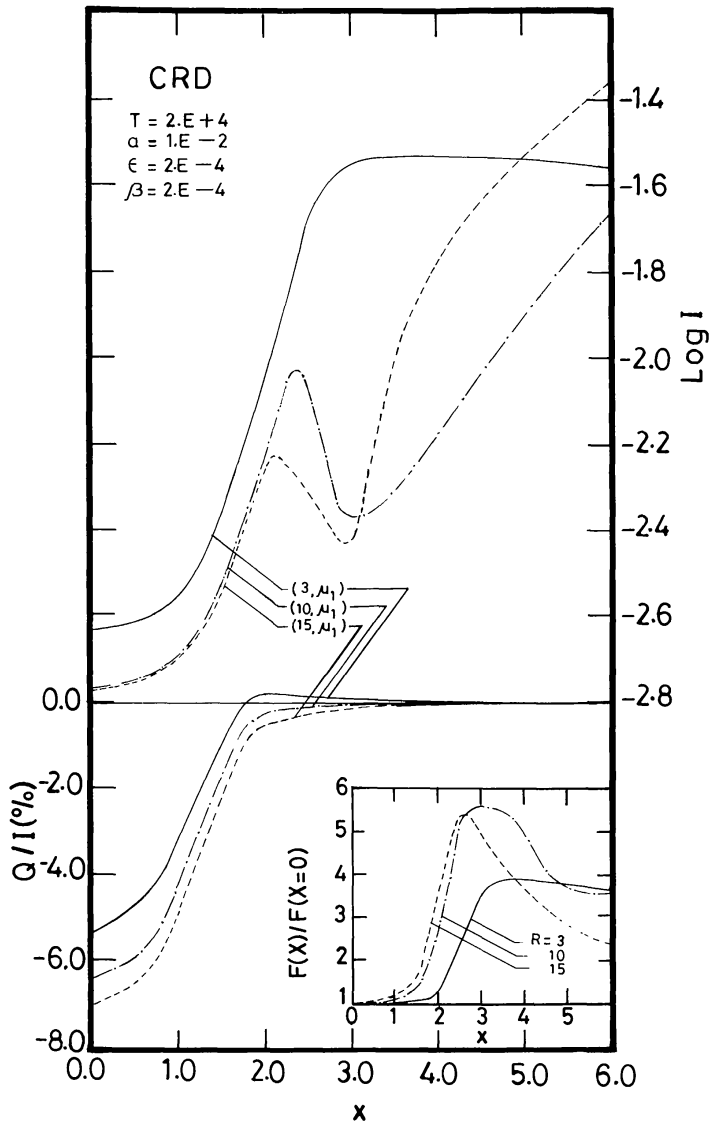

Fig. 9. Emergent specific intensity and polarization profiles in spherically-symmetric atmospheres characterized by the model parameters (T, a, ε, β) given in the figure. The R-values correspond to the extendedness of the spherical shell in terms of the stellar core radius R_C (= 1). The insert shows the disk-integrated flux profiles. The disk-integrated polarization is identically zero. CRD is the line-scattering mechanism employed.

importantly in the far-wing frequencies $x > 3.5$, there is reduction in the degree of polarization in a ring situated after the impact parameter value of $h \sim 2.4$, before it increases sharply for higher values of h. This occurs due to the opacity effect: namely, that a constant opacity case is more similar to the PP case. It is important to note that the degree of polarization in this case is also quite high. This is partly because of the smaller optical depth compared to the model representing Figures 9 and 10, and partly because of the nature of scattering: namely CS, which does not couple the different frequency points in the line during the process of scattering.

© Kluwer Academic Publishers • Provided by the NASA Astrophysics Data System

1989Ap&SS.154..119N

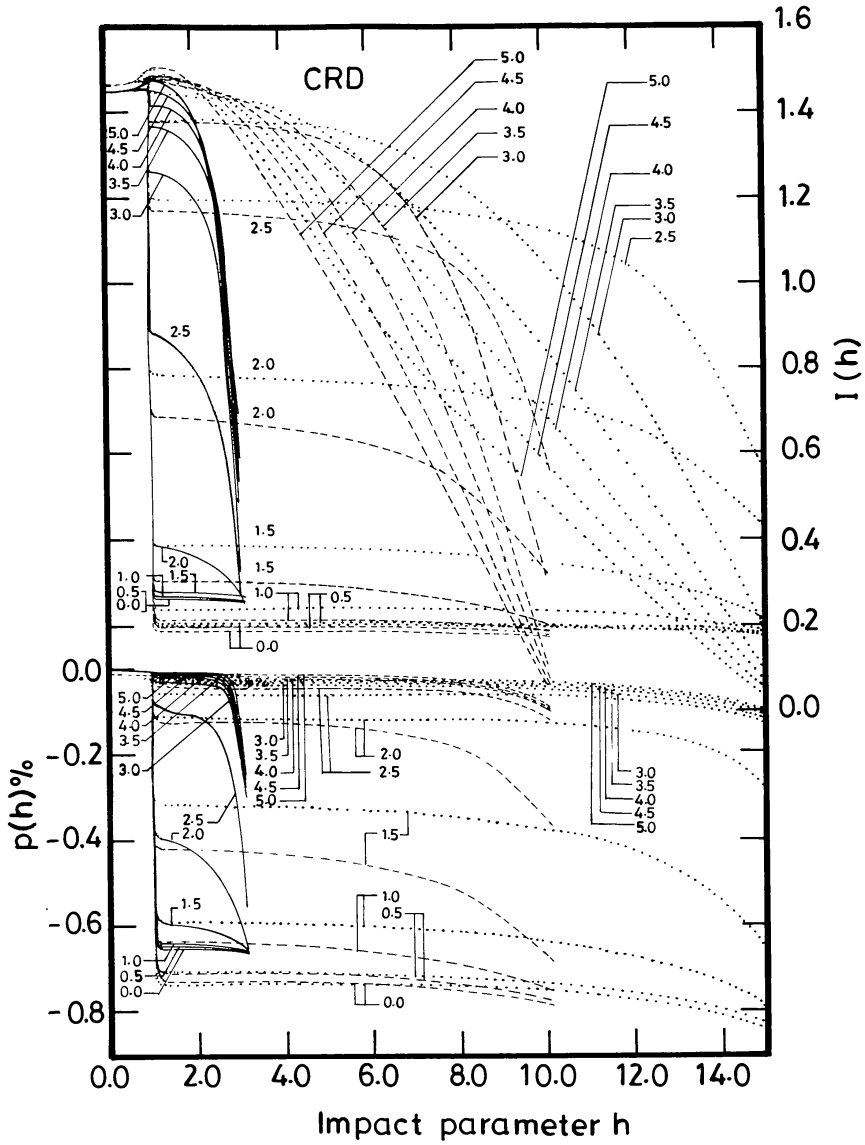

Fig. 10. The distribution of intensity $I(h)$ and polarization $p(h)$ on the apparent disk of extended spherical atmospheres. The impact parameter h is the perpendicular distance (in the units of R_C) from the centre of the apparent stellar disk. An axial-symmetry prevails about the line joining the circular disk centre, and the observer. The model parameters are the same as those of Figure 9. Three values of the extension (R) are used. The full lines ($R = 3$), dashed lines ($R = 10$), and dotted lines ($R = 15$) correspond to these cases. The numbers near the curves represent the frequency points in the bandwidth of the line profile.

4. Conclusions

Through simple schematic models, we have discussed the importance of extension of the atmosphere in polarized line-transfer problems in spherical geometry. It is found that the extension of the spherical atmosphere substantially affects the emergent intensity and polarization irrespective of the nature of the scattering. However, it is clear that PRD is the more realistic and correct mechanism of the two-level atom polarized line

© Kluwer Academic Publishers • Provided by the NASA Astrophysics Data System

1989Ap&SS.154..119N

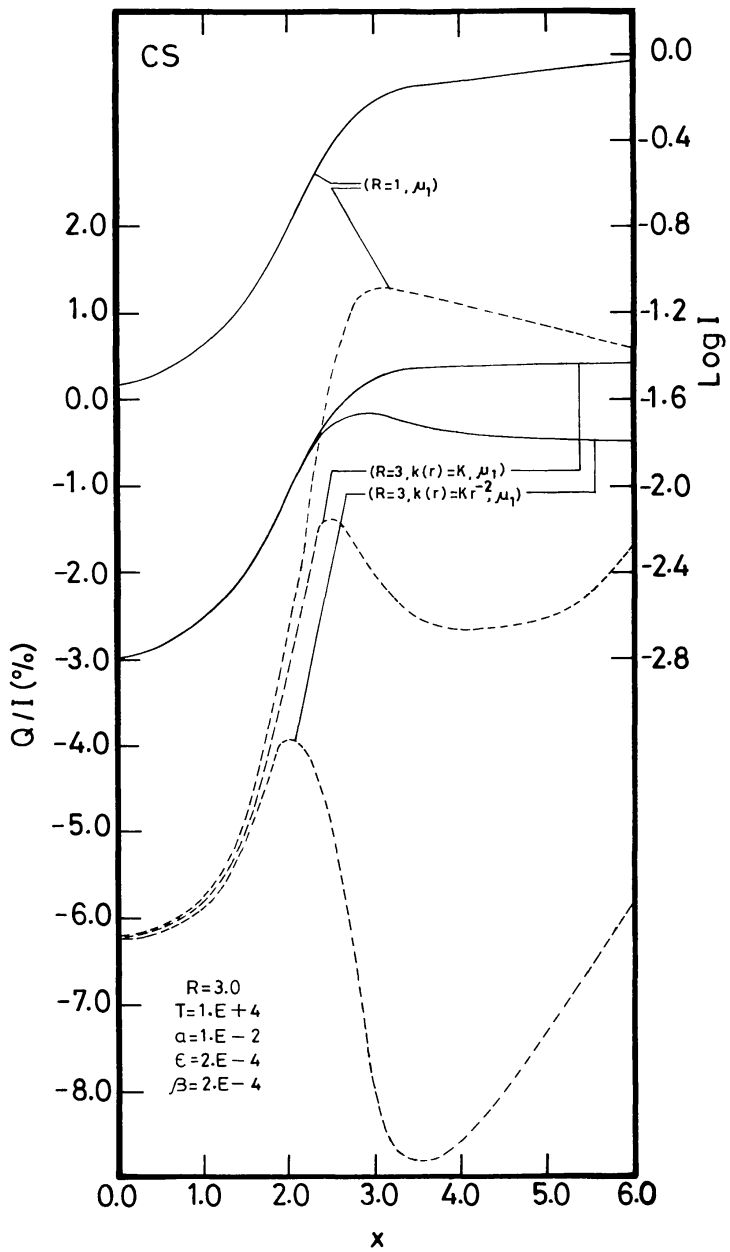

Fig. 11. Emergent specific intensity and polarization profiles for the model (T, a, ε, β) shown in the figure. Profiles for the constant opacity $k(r) = K$ and inverse-square opacity $k(r) = Kr^{-2}$ variations in the spherical models are shown. CS is the line-scattering mechanism.

transfer calculations, as compared to other two mechanisms: namely, CRD and CS. Polarization in the line profile is a sensitive indicator of the physical parameters of the model used in the calculations. However, for high optical depths (or semi-infinite atmosphere problems) the polarization profiles are less conspicuous, and do not differ very much for different opacity laws or different line-scattering models. This indicates that it is easy to model polarization of optically thick resonance lines, formed in atmospheres with smaller extensions. The disk resolved observations of spherical or

© Kluwer Academic Publishers • Provided by the NASA Astrophysics Data System

1989Ap&SS.154..119N

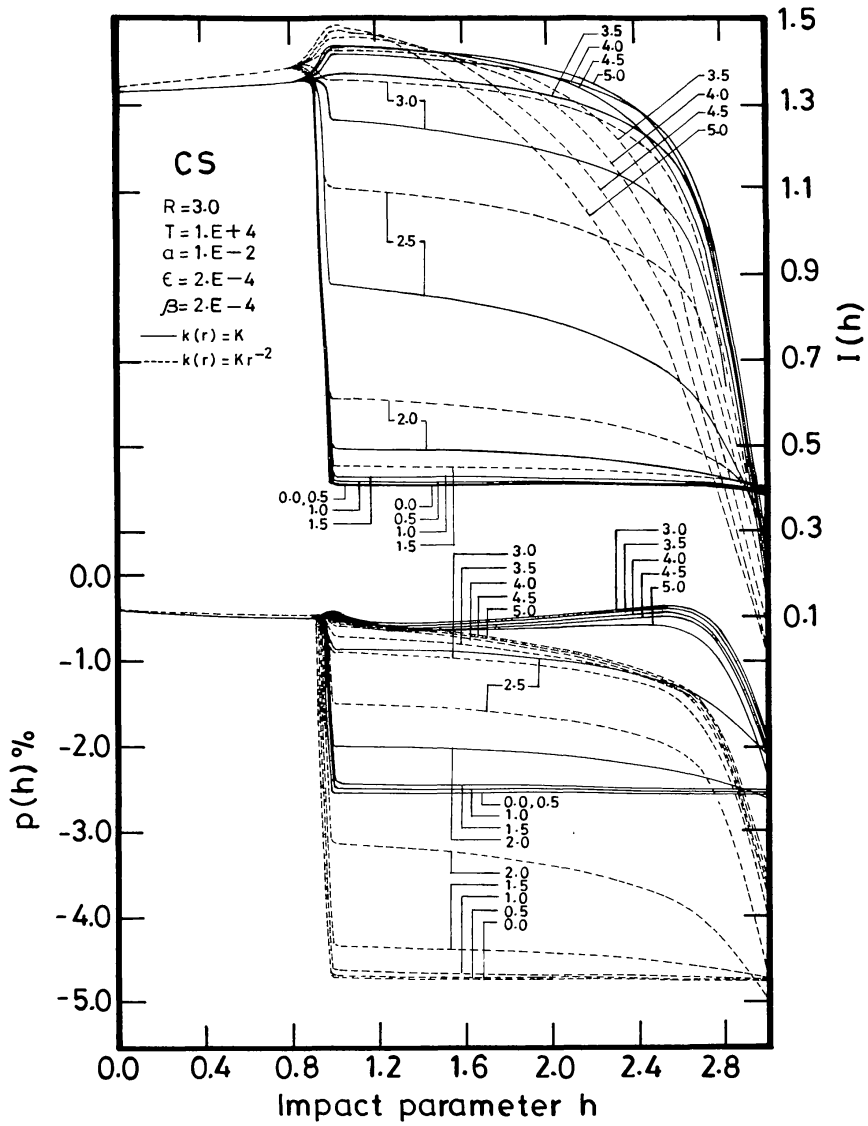

Fig. 12. A comparison of $I(h)$ and $p(h)$ computed for constant opacity and inverse-square opacity variations in model shown in Figure 11. The numbers near the curves represent the frequency points in the bandwidth of the line profile.

even non-spherical extended atmospheres (to a certain approximation) can be modelled using resonance line transfer solutions in spherical geometry. The solutions obtained for static models serve as good reference points for future calculations involving polarized line transfer in extended and expanding stellar atmospheres.

References

Ballagh, R. J. and Cooper, J.: 1977, *Astrophys. J.* **213**, 479.

Chandrasekhar, S.: 1960, *Radiative Transfer*, Dover, New York.

Cropper, M., Bailey, J., McCowage, Cannon, R. D., Couch, W. J., Walsh, J. R., Strade, J. O., and Freeman, F.: 1988, *Monthly Notices Roy. Astron. Soc.* **231**, 695.

Domke, H. and Hubený, I.: 1988, *Astrophys. J.* **334**, 527.

© Kluwer Academic Publishers • Provided by the NASA Astrophysics Data System

1989Ap&SS.154..119N

Dumont, S., Omont, A., Pecker, J. C., and Rees, D. E.: 1977, *Astron. Astrophys.* **54**, 675.
Faurobert, M.: 1987, *Astron. Astrophys.* **178**, 269.
Faurobert, M.: 1988, *Astron. Astrophys.* **194**, 268.
Hubený, I.: 1985, *Astron. Astrophys.* **145**, 461.
Linsky, J. L.: 1987, in *Radiative Properties of Hot Dense Matter III*, p. 333.
McKenna, S. J.: 1984, *Astrophys. Space Sci.* **106**, 283.
McKenna, S. J.: 1985, *Astrophys. Space Sci.* **108**, 31.
Mihalas, D.: 1978, *Stellar Atmospheres*, Freeman, San Francisco.
Nagendra, K. N.: 1987, *Astron. Nachr.* **308**, 303.
Nagendra, K. N.: 1988, *Astrophys. J.* **335**, 269.
Nagendra, K. N. and Peraiah, A.: 1984, *Astrophys. Space Sci.* **104**, 61.
Nagendra, K. N. and Peraiah, A.: 1985a, *Monthly Notices Roy. Astron. Soc.* **214**, 203.
Nagendra, K. N. and Peraiah, A.: 1985b, *Astrophys. Space Sci.* **117**, 121.
Nagendra, K. N. and Peraiah, A.: 1987, *Astron. Astrophys.* **181**, 71.
Peraiah, A.: 1984, in W. Kalkofen (ed.), *Methods in Radiative Transfer,* Cambridge University Press, Cambridge, p. 281.
Rees, D. E. and Saliba, G.: 1982, *Astron. Astrophys.* **115**, 1.
Stenflo, J. O., Bauer, T. G., and Elmore, D. F.: 1980, *Astron. Astrophys.* **84**, 60.
Streater, A., Cooper, J., and Rees, D. E.: 1988, *Astrophys. J.* **335**, 503.

© Kluwer Academic Publishers • Provided by the NASA Astrophysics Data System